Photonic Crystal Slabs for Biosensing

S. Jahns, F. von Oertzen, T. Karrock, Y. Nazirizadeh, and M. Gerken
Institute of Electrical and Information Engineering, Christian-Albrechts-Universität zu Kiel, Germany

Abstract— We investigated the functionalization of photonic crystals slabs with aptamers for the label-free detection of biomolecules. Photonic crystal slabs are slab waveguides with a periodic nanostructure that supports quasi guided modes coupling to far field radiation. Measurements were performed with light at normal incidence to the photonic crystal slab. The influence of the nanostructure duty cycle as well as the high index layer thickness is investigated for the surface and the bulk sensitivity. Nanoimprint lithography with subsequent deposition of a high index layer and biofunctionlization is presented as one approach for fabricating photonic crystal slab biosensors. In comparison photonic crystal slabs fabricated by injection-molding are considered. Oblique angle layer deposition is introduced as a means to achieve structured high index layers. Results obtained with wavelength dependent measurements are compared to simple intensity measurements in a particular wavelength range. Both methods are applicable for label-free detection. In a spectrometer-free setup we measured the binding kinetics of a 250 nM solution of the protein thrombin to the photonic crystal surface functionalized with aptamers.

1. INTRODUCTION

Label-free and compact biosensors get more and more in focus for point-of-care applications. Typically, they consist of a selective biological recognition component (receptor) connected directly with the transducer [1, 2]. The transducer transforms the binding kinetics into a detectable signal. Depending on the type of transducer the signal can be detected by, e.g., an electrochemical, colorimetric, or optical read-out system [3–5]. Using photonic crystal slabs (PCS) as the base platform for biosensors a label-free, sensitive, compact and cost-efficient system may be realized [6–8]. PCS are waveguides with a periodic nanostructure in a high refractive index material. Due to the nanostructure quasi guided modes form and may couple to far-field radiation. These modes can be excited in transmission as well as in reflection measurements and are the origin of guided mode resonances (GMR) in the optical spectrum. The quasi guided modes in the high-index layer have an evanescent fraction propagating above the PCS surface. This evanescent fraction interacts with the sample volume close to the PCS surface and produces a shift in the spectrum of the GMR caused by a refractive index change due to a mass change on the surface. By functionalizing the surface with, e.g., aptamers the protein binding kinetics results in a wavelength shift of the GMR, which may be tracked in real time with an optical read-out system [11–13]. Especially the sensitivity of the PCS to mass changes on its surface is an important factor in realizing sensitive protein detection in the pM range. Thus, in the design of PCS for protein binding the sensitivity to small refractive index changes in a thin layer above the surface needs to be optimized. This "surface sensitivity" requires a different optimal structure compared to the bulk sensitivity. Therefore, we investigated the influence of the duty cycle of the nanostructure as well as the influence of the high refractive index layer thickness. Additionally, a new approach to optimize the surface sensitivity is given by structuring the high refractive index layer using oblique angle deposition. Finally, we demonstrate label-free detection of 250 nM thrombin with our sensor using first a spectrometer based and then a compact camera based measuring setup.

2. FABRICATION OF PHOTONIC CRYSTAL SLABS

We realized photonic crystal slabs via UV nanoimprint lithography. First, the nanostructure is transferred from a glass master into a stamp consisting of polydimethylsiloxane (PDMS). Sylgard 184 and Curing Agent (*DOW Corning*) were mixed in a ratio of 8 : 1 for 15 minutes in a mixing tube (*IKA*). Then the PDMS is poured over the glass master placed within a teflon adapter. This is followed by a 15-minute evacuation inside a vacuum chamber to remove all bubbles from the PDMS. Afterwards, the PDMS is hardened in an oven at 130°C for 20 minutes. When the PDMS is hardened, it is cut out of the adapter and is pulled off the glass master. The glass master and thus the fabricated PCS have a period $\Lambda = 400\,\text{nm}$, a structure depth $t = 150\,\text{nm}$, and a duty cycle of 40 : 60.

For sample fabrication $25 \times 25\,\text{mm}^2$ glass substrates with a thickness of 1 mm were cleaned with acetone and isopropanol for 15 minutes each in an ultrasonic bath and then were dehydrated on

a hotplate at 160°C for 10 minutes. After dehydration the glass substrates are cooled down for 2 minutes before 150 µl of Amoprime (*AMO GmbH*) are spin coated for 30 seconds at 3000 rpm onto the substrates to generate a 200-nm adhesive layer. Thereafter, the substrates were baked on a hotplate for 2 minutes at 115°C und cooled down for another 2 minutes. Now 150 µl of the photoresist Amonil (*AMO GmbH*) are spin coated with the same parameters as used before. To transfer the nanostructure into the photoresist the PDMS stamp is pressed carefully into the resist and the resist is hardened for 1 minute with a UV halogen lamp with the stamp on top. After that the PDMS stamp was pulled off the resist layer and the high refractive index layer of silicon monoxide (SiO_x) was deposited by thermal evaporation. By positioning the substrates at different oblique angles we achieved angle-dependent deposition layers [10].

Another way to fabricate PCS is to use injection molding for nanostructured nickel mold replication and sputtering for the high refractive index layer. As described in detail in [9] a process has been demonstrated, in which the nanostructured nickel mold master was assembled to an adapter und positioned into a two-part injection-molding tool. 245°C hot PMMA was injected into a down to 0.4 mbar evacuated and 135°C warm injection molding tool. After cooling down to 45°C the molding tool was opened and the nanostructured PMMA was baked once again avoiding unwanted polarization rotation caused possibly by residual mechanical stress inside the material. In the last fabrication step the nanostructured PMMA was deposited with tantalum pentoxide (Ta_2O_5) via reactive sputtering.

3. DESIGN OPTIMIZATION

3.1. Duty Cycle and Layer Thickness

Sensitivity measurements were performed by evaluating transmission spectra. The PCS was placed on a microscope plate between two crossed polarization filters as described in [9]. The halogen lamp of the microscope was used as excitation source. In this measurement configuration only light interacting with the quasi-guided modes is transferred to the objective of the microscope, which is coupled to a spectrometer. The surface of the PCS was covered sequentially with two liquids with two different refractive indices to determine the bulk sensitivity. Changing the refractive index (Δn) from $n = 1.33$ (water) to $n = 1.38$ (glycerol-water-solution) above the PCS surface results in a shift ($\Delta\lambda$) of the guided mode resonance (GMR) detectable with a spectrometer. To calculate the bulk sensitivity $\Delta n/\Delta\lambda$ the shift of the resonance with the highest intensity was tracked.

For determining the surface sensitivity we first measured the GMR with water as the surrounding medium. Then we evaporated a 25 nm thick lithium fluoride (LiF) layer with a refractive index of $n = 1.39$ on top of the fabricated PCS and repeated the measurement. The surface sensitivity was then calculated by comparing both resonance wavelengths and dividing the resonance shift by the refractive index difference of water and LiF.

With these characterization methods and using the PCS fabricated with the injection-mold process we investigated the influence of the duty cycle and the layer thickness on the bulk as well as on the surface sensitivity. The bulk sensitivities range from 31.5 nm/RIU (RIU = refractive index unit) for a duty cycle of 0.2 and a high-index layer thickness of 301 nm to 138 nm/RIU for a duty cycle of 0.7 and a high-index layer thickness of 99 nm. This is a 4.38 fold enhancement. As Figure 1 shows, a high refractive index layer thickness of 99 nm causes a maximum for both sensitivities. But comparing the results of the duty cycle the maximum of the surface sensitivity is obtained for a duty cycle of 0.5 whereas a duty cycle of 0.7 causes a maximum for the bulk sensitivity. As shown by Nazirizadeh et al. [8], the mode is pulled up to the analyte area until it passes a state, where it has a maximum interaction area with the surface of the nanostructure. This may explain the differing behavior of the surface sensitivity.

3.2. Oblique Angle Deposition

Another approach to enhance the surface sensitivity is to structure the high refractive index layer additionally by oblique angle deposition. Here, we used first the finite difference time domain (FDTD) to simulate the behavior of the surface and bulk sensitivities corresponding to various deposition angles. In the simulations the sensitivities are calculated for the cases described in the last section. In Figure 2 the bulk (a) and the surface (b) sensitivities are plotted as a function of the high-index layer thickness and the deposition angle. The maximum of 93 nm/RIU for the bulk sensitivity at a deposition angle of 0° is obtained for a layer thickness of 125 nm. Changing the deposition angle to be 10° causes an improvement of 7% for the bulk sensitivity keeping the layer thickness constant. In contrast, for the surface sensitivity the maximum value of 58 nm/RIU for a

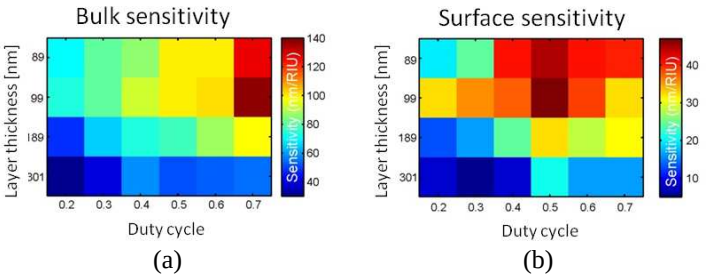

Figure 1: Results of (a) bulk and (b) surface sensitivity measurements as a function of duty cycle and layer thickness.

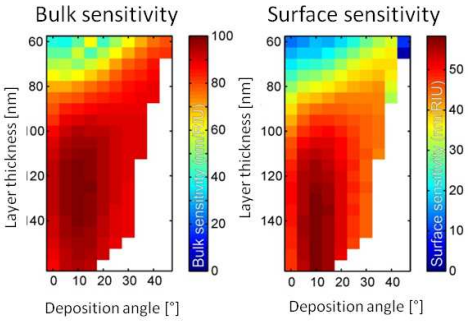

Figure 2: Simulation results of (a) bulk and (b) surface sensitivity as a function of layer thickness and deposition angle.

layer thickness of 135 nm and a deposition angle of 10°. This corresponds to a 16% enhancement compared to the normal incidence deposition. For the bulk sensitivity the simulated results were confirmed with experimental results as shown in [10].

4. PHOTONIC CRYSTALS AS BIOSENSORS

4.1. Protein Detection with Spectrometer

First, we functionalized the surface of PCS fabricated via nanoimprint lithography with thrombin binding aptamers [10]. We tested the PCS sensor within a fluid cell by evaluating the resonance wavelength shift during thrombin binding with a spectrometer setup. We use the same spectrometer setup as described in chapter III. A. For Figure 3 the peak wavelength of the GMR was tracked over time. To generate a baseline a neutral tris-HCl-buffer (pH 7.4) is filled inside the fluid cell. After 10 minutes the pure buffer is replaced by a 250 nM thrombin-buffer solution. Due to thrombin association to the surface of the PCS the wavelength increases until all aptamers are saturated with thrombin. Washing again with pure buffer the unbound thrombin is washed away and the wavelength decreases a bit. Regeneration of the sensor was achieved by replacing the pure buffer with slightly acid buffer. This caused a different folding of the aptamers and therefore a dissociation of the bound thrombin. As shown we can repeat this measuring sequence with nearly the same results. The association, dissociation, and regeneration kinetics of 250 nM thrombin are clearly visible in the wavelength shift of the GMR.

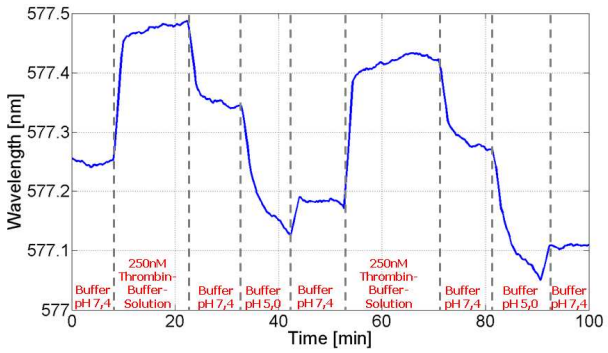

Figure 3: Resonance wavelength shift resulting from association, dissociation and regeneration kinetics of 250 nM thrombin solution.

4.2. Protein Detection without Spectrometer

Next we investigated a measurement configuration without a spectrometer. This spectrometer-free setup is particularly promising for parallel detection of many functionalized spots with a camera. The wavelength shift is transformed into an intensity change using a colored light emitting diode (LED) as excitation source and again crossed polarization filters. The resulting intensity change may be observed with a simple CMOS sensor of a camera [12] or a photodiode [13].

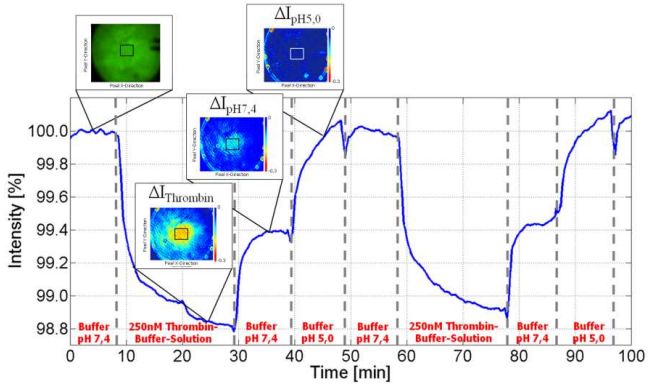

Figure 4: Association, dissociation and regeneration kinetics of 250 nM thrombin solution observed without spectrometer.

Initially, the thrombin detection was repeated with the same measuring sequence mentioned before using the camera setup. Figure 4 shows the intensity values corresponding also to the association, dissociation and regeneration kinetics. The wavelength increase results in an intensity reduction and the wavelength decrease in an intensity increase.

5. CONCLUSION

We investigated different design possibilities to improve the sensitivity of a PCS biosensor. By varying the duty cycle and the layer thickness of the PCS we identified a duty cycle of 0.5 and a layer thickness of 99 nm as optimal values for a high surface sensitivity. Depositing the high-index layer with the substrates tilted to 10° improves the surface sensitivity additionally. Furthermore, a label-free detection of 250 nM thrombin was demonstrated with a spectrometer setup as well as with a compact and spectrometer-free camera setup. Particularly the camera-based configuration has a high miniaturization potential paving the way towards smartphone biosensing. This approach is promising for mobile biosensors applicable, for example, for home diagnostics.

ACKNOWLEDGMENT

The authors acknowledge support by the German Federal Ministry of Education and Research (BMBF) within the project BioCard (0316145B).

REFERENCES

1. Scheller, F., et al., *Cur. Opt. Biotechnol.*, Vol. 12, 35–40, 2001.
2. Qureshi, A., et al., *Sens. Actuat. B*, 62–76, 171–172, 2012.
3. Wang, Y., et al., *Chem. Commun.*, Vol. 22, 2520–2522, 2008.
4. Jung, L., et al., *Sens. Actuat. B*, Vol. 129, 372–379, 2008.
5. Lifson, M. A., et al., *Anal. Chem.*, Vol. 86, 1016–1022, 2014.
6. Magnusson, R., et al., *Sensors*, Vol. 11, 1476–1488, 2011.
7. Han, J., et al., *Anal. Chem.*, Vol. 85, 3104–3109, 2013.
8. Threm, D., et al., *Journal of Biophotonics*, Vol. 5, Nos. 8–9, 601–616, 2012.
9. Nazirizadeh, Y., et al., *Opt. Mater. Express*, Vol. 3, 556–565, 2013.
10. Nazirizadeh, Y., et al., *Opt. Express*, Vol. 21, 18661–18670, 2013.
11. Lin, S.-F., et al., *Sensors*, Vol. 11, No. 9, 8953–8965, 2011.
12. Jahns, S., et al., *Proc. IEEE Sensors*, Baltimore, USA, 2013.
13. Nazirizadeh, Y., et al., *Opt. Express*, Vol. 18, 19120–19128, 2010.